

**Density functional theory study of platinum oxides: From infinite crystals to nanoscopic particles**

N. Seriani\*

*Institut für Werkstoffwissenschaft, Technische Universität Dresden, Hallwachsstrasse 3, 01069 Dresden, Germany  
and Institut für Materialphysik, Universität Wien, Sensengasse 8, A-1090 Wien, Austria*

Z. Jin

*Laboratory of Special Functional Materials, Henan University, Kaifeng 475001, China*

W. Pompe

*Institut für Werkstoffwissenschaft, Technische Universität Dresden, Hallwachsstrasse 3, 01069 Dresden, Germany*

L. Colombi Ciacchi

*Theory of Condensed Matter Group, Cavendish Laboratory, J J Thomson Avenue, Cambridge CB3 0HE, United Kingdom;**Fraunhofer Institut für Werkstoffmechanik, Wöhlerstrasse 11, 79108 Freiburg, Germany;**and Institut für Zuverlässigkeit von Bauteilen und Systemen, Kaiserstrasse 12, 76131 Karlsruhe, Germany*

(Received 11 January 2007; revised manuscript received 8 September 2007; published 19 October 2007)

For over a century, platinum oxides find technologically relevant applications in various fields ranging from catalysis to electrochemistry and nanoelectronics. We have performed a density functional theory study of the PtO, Pt<sub>3</sub>O<sub>4</sub>, and PtO<sub>2</sub> bulk oxide phases. In our calculations, PtO and Pt<sub>3</sub>O<sub>4</sub> present metallic character at the simple generalized gradient approximation level. The application of Hubbard corrections to the Kohn-Sham Hamiltonian opens a small gap in the electronic band structure of PtO, but not of Pt<sub>3</sub>O<sub>4</sub>, in which metallic Pt-Pt bonds are revealed by a Bader analysis of the calculated electronic structure. These results, together with the noninteger oxidation number of the Pt ions, are indicative of metallicity of the Pt<sub>3</sub>O<sub>4</sub> phase which may be consistent with the known metallic character of platinum bronzes. Moreover, we have calculated the relative thermodynamic stabilities of platinum oxide Wulff's particles and discussed the results in the context of catalysis. Finally, we have predicted that the formation of  $\alpha$ -PtO<sub>2</sub> nanotubes could be energetically feasible. This result is of potential interest both for nanotechnological and catalytic applications and may explain the formation of curled  $\alpha$ -PtO<sub>2</sub> sheets observed in high-resolution transmission electron microscopy images.

DOI: [10.1103/PhysRevB.76.155421](https://doi.org/10.1103/PhysRevB.76.155421)

PACS number(s): 61.46.-w, 71.20.-b, 71.15.-m, 82.60.-s

**I. INTRODUCTION**

Historically, interest in the structure and properties of platinum oxides arose in the second half of the 19th century from the observed reactivity of the generally inert platinum metal under particularly aggressive chemical conditions.<sup>1</sup> A series of early studies on the crystal structures and the thermodynamical stabilities of different oxides<sup>2-6</sup> culminated in the clear identification of five pure platinum oxide phases, namely, PtO, Pt<sub>3</sub>O<sub>4</sub>,  $\alpha$ -PtO<sub>2</sub>,  $\beta$ -PtO<sub>2</sub>, and  $\beta'$ -PtO<sub>2</sub>, as well as a large number of platinate compounds. The existence of other bulk structures, such as Pt<sub>2</sub>O (Ref. 7) or Pt<sub>3</sub>O<sub>8</sub>,<sup>5</sup> remains uncertain. The technological importance of platinum oxides is large and multifold and covers fields of application ranging from catalysis to electrochemistry and nanoelectronics. In particular, the catalytic activities of platinum oxides have been investigated for more than a century (see, e.g., Ref. 8 and references therein). Modern examples of applications comprise the catalytic hydrosilylation of functionalized alkenes<sup>9</sup> and aryl alkynes,<sup>10</sup> the oxidation of ethanol to acetic acid,<sup>11</sup> and the oxidation of ammonia to nitrogen(II) oxide.<sup>12</sup> Finally, superficial oxide phases can form on platinum nanoparticles under oxidizing conditions (e.g., in automobile catalysts) and may trigger the oxidation of carbon compounds according to Mars-van Krevelen reaction mechanisms.<sup>13,14</sup>

In electrochemical applications involving platinum electrodes, the formation of a thin oxide film on the metal surface affects the mechanism and kinetics of various anodic processes (see Ref. 15 and references therein). As a particular case, superficial oxidation of platinum-based electrochemical biosensors influences the adsorption mode of protein probes on the electrode's surface.<sup>16</sup> In nanoelectronics, thin films of (amorphous) platinum oxides find application as electrodes for memory capacitors<sup>17,18</sup> and in super-resolution near-field structure disks.<sup>19,20</sup> The versatility of PtO<sub>x</sub> films lies above all in the possibility of tuning the electronic properties of the films with the film deposition conditions.<sup>21,22</sup> Depending on their structure and composition, platinum oxide films present metallic, semiconducting, or insulating behavior, with the latter being particularly evident in the case of fully oxidized PtO<sub>2</sub> films.<sup>21,23</sup> This variability of the physical properties of platinum oxides has been known for long time (as reviewed, for instance, in Ref. 24). A class of compounds with the generic formula M<sub>x</sub>Pt<sub>3</sub>O<sub>4</sub> (platinum bronzes) appears to be particularly interesting, where M is an alkali or transition metal and 0 ≤ x ≤ 1.<sup>25-27</sup> Most of these compounds present clear metallic character as a combined consequence of their structure, where square-planar PtO<sub>4</sub> motifs are stacked in infinite columns with Pt-Pt distances of ~2.85 Å, and of their noninteger oxidation state, indicative of delocalized electrons. A particular case is represented by pure Pt<sub>3</sub>O<sub>4</sub>, which appears also to be very attractive due to its

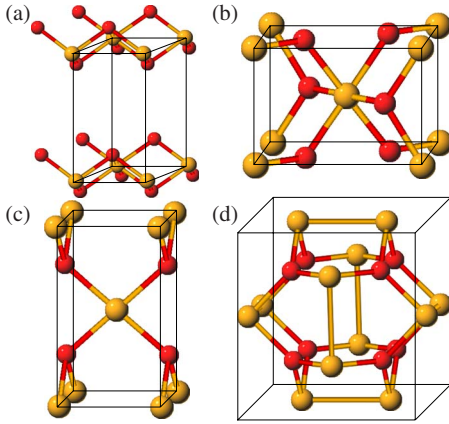


FIG. 1. (Color online) Crystal structures of the investigated Pt oxides: (a)  $\alpha$ -PtO<sub>2</sub>, (b)  $\beta$ -PtO<sub>2</sub>, (c) PtO, and (d) Pt<sub>3</sub>O<sub>4</sub>.

catalytic activity, both as a main component of the so-called Adams' catalyst<sup>28</sup> and as a superficial oxide phase potentially active toward the oxidation of carbon compounds.<sup>29</sup>

While an amount of theoretical investigations have been carried out recently to address the structure and chemical properties of thin oxide films formed on Pt surfaces in the context of catalysis,<sup>29–34</sup> computational studies on bulk platinum oxide crystals are relatively scarce. These comprise density functional theory (DFT) investigations on the thermodynamic stability of PtO<sub>2</sub> allotropes<sup>35,36</sup> and a few studies on the electronic structure of PtO.<sup>37–40</sup> In this work, we present a computational study of the PtO<sub>2</sub>, Pt<sub>3</sub>O<sub>4</sub>, and PtO platinum oxide phases, whose crystal structures are reported in Fig. 1. After a brief description of the methods employed (Sec. II), we will address the presence of metallic vs semiconducting character of PtO and Pt<sub>3</sub>O<sub>4</sub> phases at the generalized gradient approximation (GGA)+*U* level of theory, combined with a Bader's analysis of the bond properties of the solids (Sec. III). Moreover, in Sec. IV, we investigate how the finite size of nanoscopic structures influences the thermodynamic stability of the oxides. First, we study the effect of particle size on the oxidation state of ideal Wulff's particle.<sup>41</sup> Second, motivated by experimental high-resolution transmission electron microscopy (HRTEM) images of  $\alpha$ -PtO<sub>2</sub> samples, which are also reported in this paper, we investigate the possibility of formation of  $\alpha$ -PtO<sub>2</sub> nanotubes as potentially interesting structures in nanotechnological and catalytic applications. The main results will be finally summarized in Sec. V.

## II. METHODS

### A. Computational details

Total energy calculations and structural optimization of bulk structures, surfaces, and oxide nanotubes have been performed under periodic boundary conditions within the DFT using the PW91 exchange-correlation potential<sup>42</sup> and separable norm-conserving Troullier-Martins pseudopotentials,<sup>43</sup> as implemented in the LAUTREC code<sup>44,45</sup> and extensively tested in previous works.<sup>29,46,47</sup> Special *k* points for integra-

tion in the first Brillouin zone have been produced with the method of Monkhorst and Pack<sup>48</sup> and checked for convergence in all cases. Kinetic-energy cutoffs to the plane-wave wave function expansions of 50 and 70 Ry have been used for structural minimizations and total energy calculations, respectively. The Bader analysis has been performed starting from the charge density calculated with the ABINIT code using the postprocessing program AIM.<sup>49</sup> GGA+*U* calculations<sup>50,51</sup> have been performed using the QUANTUM-ESPRESSO package<sup>52</sup> using ultrasoft pseudopotentials<sup>53</sup> at a kinetic-energy cutoff of 40 Ry. Although the GGA+*U* method was originally introduced to deal with magnetic Mott-Hubbard insulators, some authors have recently applied this approach also to systems which are not strongly correlated (such as the CO molecule) as an empirical tool to correct the position of selected orbitals or bands.<sup>54,55</sup> This relies on the fact that an effect of the *U* correction is to shift fully occupied electronic states to lower energies and completely empty states to higher energies.

The Gibbs free energies of formation of the oxide phases,  $\Delta G_{\text{PtO}_x}^f$ , have been calculated combining DFT total energies and standard thermodynamic data for enthalpy and entropy of the oxygen gas<sup>56</sup> according to

$$\Delta G_{\text{PtO}_x}^f(T,p) = g_{\text{PtO}_x}^{\text{bulk}}(T,p) - g_{\text{Pt}}^{\text{bulk}}(T,p) - \frac{x}{2} g_{\text{O}_2}^{\text{gas}}(T,p), \quad (1)$$

where  $g_{\text{O}_2}^{\text{gas}}$  is the free energy of a dioxygen molecule in gas phase and  $g^{\text{bulk}}$  is the free energy of each bulk phase (calculated as in Ref. 29).

### B. Experimental details

$\alpha$ -PtO<sub>2</sub> samples were prepared as reported elsewhere.<sup>11</sup> We have considered both "as produced" samples and samples which had been annealed for 3 h at 350 °C in a N<sub>2</sub> atmosphere. High-resolution transmission electron microscopy (HRTEM) images were collected at an applied potential difference of 100 keV on a JEM-2010 electron microscope.

## III. BULK PLATINUM OXIDE PHASES

We have calculated the structural and thermodynamic properties of the PtO, Pt<sub>3</sub>O<sub>4</sub>,  $\alpha$ -PtO<sub>2</sub>, and  $\beta$ -PtO<sub>2</sub> in a previous work.<sup>29</sup> We summarize them in Table I and very briefly here below before describing the details of their electronic properties in the next couple of sections. According to the coordinations of the Pt ions in the bulk, the four oxides can be classified in two categories. The first comprises the two PtO<sub>2</sub> allotropes, in which the Pt atoms are coordinated octahedrally by six O atoms. The second comprises Pt<sub>3</sub>O<sub>4</sub> and PtO, in which the Pt atoms are coordinated by four O atoms in a square-planar geometry. In each category, the oxide structures differ from each other by the arrangement of these basic structural elements. These structural differences are also associated with profound differences in the electronic and dielectric properties of the oxides.<sup>24</sup> Fully oxidized platinum oxides are either semiconductors or insulators,<sup>21,23,35</sup> whereas oxides containing partially oxidized Pt ions in

TABLE I. Calculated physical properties of bulk platinum oxide phases. Experimental data are reported in parentheses.

	PtO <sup>a</sup>	Pt <sub>3</sub> O <sub>4</sub> <sup>b</sup>	$\alpha$ -PtO <sub>2</sub> <sup>b</sup>	$\beta$ -PtO <sub>2</sub> <sup>c</sup>
Structure	PdS, tetragonal	Simple cubic	CdI <sub>2</sub> , hexagonal	CaCl <sub>2</sub> , orthorhombic
<i>a</i> (Å)	3.10 (3.08)	5.65 (5.59)	3.14 (3.10)	4.49 (4.48)
<i>b/a</i>				1.05 (1.01)
<i>c/a</i>	1.745 (1.735)		1.85 (1.38–1.42)	0.70 (0.70)
Pt–O (Å)	2.06 (2.04)	2.00 (1.97)	2.05	2.03 (1.99)
Pt–Pt (Å)	3.10 (3.08)	2.83 (2.79)	3.14 (3.10)	3.15 (3.14)
<i>B</i> (GPa)	368	262		246 (265) <sup>d</sup>
$\Delta H_f$ (eV)	–0.76	–1.42	–2.05	–2.06
$E_{gap}$ (eV)	0.0, 0.38 <sup>e</sup>	0.0, 0.0 <sup>e</sup>	1.49	0.43

<sup>a</sup>Reference 60.

<sup>b</sup>Reference 5.

<sup>c</sup>Reference 61.

<sup>d</sup>Calculated with DFT, Ref. 35.

<sup>e</sup>GGA+U,  $U=9$  eV.

square-planar oxygen coordination are found to be metallic<sup>25–27</sup> or quasimetallic.<sup>57</sup>

The thermodynamically stable phase at low temperature is  $\alpha$ -PtO<sub>2</sub>.<sup>5</sup> At increasing temperatures, decomposition of the oxide occurs via the transitions  $\alpha$ -PtO<sub>2</sub> → Pt<sub>3</sub>O<sub>4</sub> → Pt.<sup>58,59</sup> In Ref. 29, the computed transition temperatures at 1 atm of oxygen pressure are 870 and 970 K, without including any vibrational entropy contributions to the free energy. These are roughly consistent with the measured transition temperatures of 910 and 1070 K in the case of oxidized supported nanoparticles subject to thermal annealing.<sup>58</sup> The  $\beta$  and  $\beta'$  PtO<sub>2</sub> allotropes are stable only at high temperatures and high oxygen pressures.<sup>5,6</sup>

### A. PtO<sub>2</sub> allotropes

$\alpha$ -PtO<sub>2</sub> presents a laminar crystal structure consisting of stacked O-Pt-O trilayers which are covalently bonded in plane, while the interactions between trilayers are of van der Waals type.<sup>5,32,36</sup> While a good agreement between the experimental and computed edge of the hexagonal cell could be achieved (Table I), the GGA approximation heavily underestimates the interlayer forces,<sup>62</sup> similarly as in the case of graphite.<sup>63</sup>  $\beta$ -PtO<sub>2</sub> crystallizes in an orthorhombic CaCl<sub>2</sub> structure, which is closely related to the rutile structure, differing from the latter only through a rotation of the oxygen pairs around the central Pt atom. We found that the rutile structure is metastable with respect to the CaCl<sub>2</sub> structure and lies 89 meV/f.u. higher in energy (without considering zero-point energy contribution). For the same structures, Wu and Weber found a difference of  $\sim 200$  meV without optimization of the *b/a* and *c/a* parameters.<sup>35</sup> This small energy difference is compatible with the observed phase transition which occurs at high pressures. Contrary to experimental evidence, but in agreement with previous DFT calculations,<sup>31</sup> we found that  $\alpha$ -PtO<sub>2</sub> is less stable than  $\beta$ -PtO<sub>2</sub> by about 10 meV/Pt atom. In Ref. 36, the correct stability could be recovered by taking into account the zero-point vibrational

energy differences between the two structures. In addition, destabilization of the  $\alpha$  allotrope could also be due to the underestimation of the interlayer binding energy, which, at the GGA level, amounts to only 37 meV/f.u.

The calculated electronic band structures of the  $\alpha$  and  $\beta$  allotropes reveal their semiconducting character (Fig. 2).  $\alpha$ -PtO<sub>2</sub> presents an indirect energy gap of 1.49 eV, which is to be compared with the experimental value of 1.84 eV measured in Ref. 11. The gap of  $\beta$ -PtO<sub>2</sub> is considerably smaller (0.43 eV), which is compatible with the pseudogap found in a previous DFT calculation.<sup>35</sup> The presence of a band gap in both compounds can be understood as a consequence of the octahedral oxygen coordination of the Pt(IV) ions. In such coordination, ligand-field theory predicts the  $t_{2g}$  orbitals  $d_{xy}$ ,  $d_{xz}$ , and  $d_{yz}$  to be degenerate and to lie in energy well below the  $e_g$  orbitals,  $d_{z^2}$  and  $d_{x^2-y^2}$ .<sup>64</sup> Given the formal  $d^6$  configuration of the Pt atoms, it follows that the  $t_{2g}$  states are occupied and separated in energy from the empty  $e_g$  states, thus leading to a nonmagnetic, insulating band structure.

### B. PtO and Pt<sub>3</sub>O<sub>4</sub>

As described for the first time by Moore and Pauling,<sup>2</sup> PtO crystallizes in the tetragonal PtS crystal structure and is

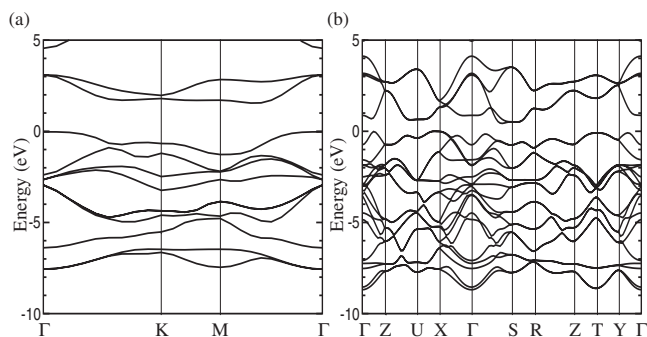


FIG. 2. Electronic band structures of (a)  $\alpha$ -PtO<sub>2</sub> and (b)  $\beta$ -PtO<sub>2</sub>. The energy values are reported relative to the valence band top.

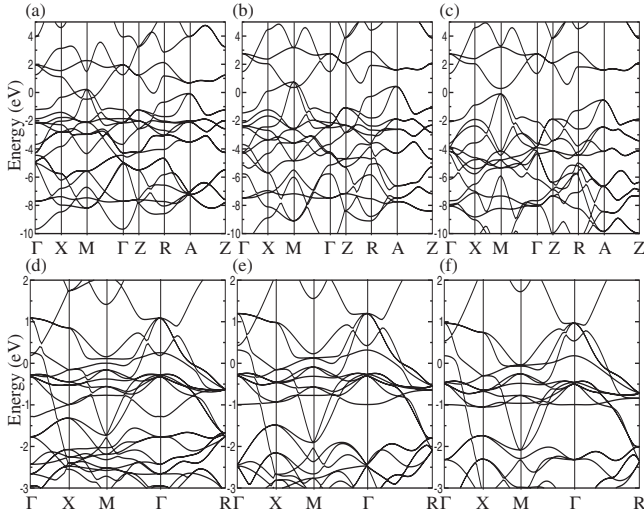


FIG. 3. Electronic band structures of PtO and Pt<sub>3</sub>O<sub>4</sub>: (a) PtO within spin-paired GGA, (b) PtO within GGA+ $U$  and  $U=4$  eV, (c) PtO within GGA+ $U$  and  $U=9$  eV, (d) Pt<sub>3</sub>O<sub>4</sub> within spin-paired GGA, (e) Pt<sub>3</sub>O<sub>4</sub> within GGA+ $U$  and  $U=4$  eV, and (f) Pt<sub>3</sub>O<sub>4</sub> within GGA+ $U$  and  $U=9$  eV. The energy values are reported relative to the Fermi level.

isostructural to the only stable palladium oxide, PdO. At the GGA level, we find a spin-paired ground state for the electronic structure of PtO, and the calculated band structure displays metallic character [Fig. 3(a)]. This finding and the qualitative shape of the band structure agree well with previous calculations where local approximations to the exchange-correlation functional have been employed.<sup>38,40</sup> The available experimental literature is scarce and describes PtO either as a poorly conducting metal<sup>57</sup> or, more reliably, as a small-gap semiconductor.<sup>60</sup> Indeed, in the most recent theoretical study available, a gap of 0.86 eV has been calculated using a hybrid functional with exact exchange.<sup>40</sup> Here, we find that the electronic band structure of PtO can be corrected, at least qualitatively, by addition of a simple Hubbard term  $U$  to the Kohn-Sham Hamiltonian.<sup>50,51</sup> Namely, at the GGA+ $U$  level, a gap of 0.38 eV ( $U=9$  eV) opens at the  $M$  point of the Brillouin zone [Fig. 3(c)], in agreement with the results in Ref. 40. As in the case of the PtO<sub>2</sub> compounds, ligand-field theory is able to qualitatively rationalize the non-magnetic insulating band structure of PtO. In this compound, the Pt ions are square-planar coordinated to four O atoms. For this geometry, ligand-field theory predicts the  $d_{x^2-y^2}$  orbital to lie considerably higher in energy than the other  $d$  orbitals,<sup>64</sup> and since Pt ions have a formal  $d^8$  configuration, this results in a gap between occupied and unoccupied states.

The situation is quite different for Pt<sub>3</sub>O<sub>4</sub>, which crystallizes in the simple cubic waserite structure.<sup>3,5,29</sup> In the GGA calculations, Pt<sub>3</sub>O<sub>4</sub> is also found to have metallic character [Fig. 3(d)], similar to PtO. However, in this case, the absence of a band gap could not be corrected at the GGA+ $U$  level. The addition of a Hubbard term up to 9 eV has a noticeable effect on the relative positions of the calculated bands [Fig. 3(f)], but the electronic structure remains metallic.<sup>65</sup> This shows that metallicity in Pt<sub>3</sub>O<sub>4</sub> is stable toward the introduction of an empirical Hubbard  $U$  term in the Hamiltonian.

Indeed, the fractional formal oxidation state of the square-planar coordinated Pt ions is expected to lead to partial occupation of the  $d$  states within ligand-field theory,<sup>64</sup> without considering hybridization between neighboring Pt ions. Thus, the computed metallicity may not originate only from an error in the position of the  $d$  states, as in PtO, but could be an intrinsic feature of this compound.

### C. Bader analysis of bulk platinum oxides

In this section, we analyze the interactions between atoms in the various platinum oxide phases by using the “atoms in molecules” theory originally developed by Bader.<sup>66</sup> In Bader’s approach, point charges on the atoms are calculated as the difference between the nuclear charges and the integrated electron density in the regions of space belonging to each atom (atomic basins). These regions are defined by the envelope of surfaces through which the flux of the gradient of the electron density  $\nabla\rho$  is zero. For the oxide phases described in the previous sections, we found that the calculated Bader charges on the Pt atoms (in units of the electron charge) are roughly proportional to the nominal value of the oxidation state of the Pt ion: 1.53 for  $\alpha$ -PtO<sub>2</sub>, 1.62 for  $\beta$ -PtO<sub>2</sub>, 1.13 for Pt<sub>3</sub>O<sub>4</sub>, and 0.86 for PtO. For the O atoms, the charges remain roughly constant:  $-0.76$  for  $\alpha$ -PtO<sub>2</sub>,  $-0.81$  for  $\beta$ -PtO<sub>2</sub>,  $-0.85$  for Pt<sub>3</sub>O<sub>4</sub>, and  $-0.86$  for PtO.

The existence of chemical bonds can be inferred by the presence of saddle points of the electron density  $\rho$  between pairs of atoms, the so-called bond critical points  $\mathbf{r}_c$ . At  $\mathbf{r}_c$ , bond properties can be quantified by the values of the electron density and of its Laplacian, which can be expressed as the sum of the eigenvalue of the Hessian of the density,  $\lambda_1 + \lambda_2 + \lambda_3 = \nabla^2\rho$ . For instance, the ratio between the more negative and the positive eigenvalues of the Hessian of the density,  $|\lambda_2|/\lambda_3$ , indicates to which extent the electron density is spread away from the internuclear bond. The higher this ratio, the softer the bond.<sup>67,68</sup> If the bond is metallic, this can also be considered as a qualitative indicator of the bond metallicity.<sup>67</sup> Metallicity of a bond, however, is better characterized by the ratio  $\xi = \rho(\mathbf{r}_c)/\nabla^2\rho(\mathbf{r}_c)$ .<sup>67</sup> Namely, values of  $\xi$  considerably lower than 1.0 indicate nonmetallic bonds, whereas values close to unity indicate metallic bonds. Moreover, covalent and ionic interactions can be distinguished by the kinetic energy per electron at the bond critical point, i.e., the ratio between the kinetic-energy density  $G(\mathbf{r}_c)$  and the density  $\rho(\mathbf{r}_c)$  itself.<sup>69</sup>  $G(\mathbf{r}_c)/\rho(\mathbf{r}_c)$  should be less than 1.0 for covalent interactions and larger than 1.0 for ionic interactions. In the internuclear region, the slow variation of the density allows us to write the kinetic-energy density as a series expansion around the Thomas-Fermi result:<sup>69,70</sup>  $G(\mathbf{r}_c) = 2.8713[\rho(\mathbf{r}_c)]^{5/3} + \nabla^2\rho(\mathbf{r}_c)/6$ , where all quantities are expressed in a.u.

As reported in Table II, we found that the Pt-O bonds in all oxide phases are clearly of ionic nature [the ratios  $G(\mathbf{r}_c)/\rho(\mathbf{r}_c)$  are always larger than 1.0] and similar across the different phases. As far as Pt-Pt interactions are concerned, we have found the presence of Pt-Pt bond critical points not only in metallic platinum but also in PtO and Pt<sub>3</sub>O<sub>4</sub>. In both PtO<sub>2</sub> phases, where the Pt-Pt distances are about 3.15 Å, no

TABLE II. Bader analysis results for the bond critical points: density  $\rho$ , Laplacian of the density  $\nabla^2\rho(r)$ , their ratio  $\xi$ , eigenvalues of the Hessian [ $\nabla^2\rho(r)=\sum_i\lambda_i$ ], estimated kinetic energy  $G$  (see text), and ratio kinetic energy/density. All quantities in a.u.

	$\rho(\mathbf{r}_c)$	$\nabla^2\rho(\mathbf{r}_c)$	$\xi$	$\lambda_1$	$\lambda_2$	$\lambda_3$	$ \lambda_2 /\lambda_3$	$G(\mathbf{r}_c)$	$G(\mathbf{r}_c)/\rho(\mathbf{r}_c)$
Pt–O									
$\alpha$ -PtO <sub>2</sub>	0.120	0.346	0.347	-0.142	-0.165	0.653	0.253	0.141	1.175
$\beta$ -PtO <sub>2</sub>	0.121	0.381	0.318	-0.142	-0.162	0.685	0.236	0.148	1.223
Pt <sub>3</sub> O <sub>4</sub>	0.128	0.436	0.294	-0.150	-0.157	0.743	0.211	0.166	1.297
PtO	0.107	0.381	0.281	-0.072	-0.130	0.583	0.223	0.133	1.243
Pt–Pt									
Pt <sub>3</sub> O <sub>4</sub>	0.051	0.059	0.864	-0.038	-0.040	0.137	0.291	0.030	0.588
PtO	0.029	0.044	0.659	-0.019	-0.019	0.082	0.231	0.015	0.517
Pt	0.052	0.079	0.658	-0.028	-0.034	0.141	0.241	0.034	0.654

Pt-Pt bond critical point has been found. In PtO, uninterrupted rows of Pt-Pt bonds run along the  $a$  and  $b$  axes of the tetragonal unit cell [Fig. 4(a)]. The Pt-Pt distance is 3.10 Å, and  $\rho(\mathbf{r}_c)$  is about 60% of the corresponding value in metallic platinum (Table II). In Pt<sub>3</sub>O<sub>4</sub>, Pt-Pt bond rows run along all three crystallographic directions. The computed Pt-Pt distance is only 2.83 Å, very similar to that in metallic platinum (2.82 Å). Accordingly, the  $\rho(\mathbf{r}_c)$  values of the Pt-Pt bonds are nearly the same in both cases (Table II). The other Bader indicators suggest that the Pt-Pt bond in Pt<sub>3</sub>O<sub>4</sub> is also the softest (highest  $|\lambda_2|/\lambda_3$ ) and the most metallic (highest  $\xi$ ).

It is noticeable that the analysis above reveals the presence of metallic Pt-Pt bonds aligned in infinite rows in PtO and Pt<sub>3</sub>O<sub>4</sub>, for which no gap in the electronic band structure has been found in our GGA calculations. In the case of PtO, this seems to be an artifact of the local exchange-correlation functional, which could be corrected by addition of an empirical Hubbard term in the Kohn-Sham Hamiltonian. However, the Hubbard correction is not able to open a gap in the band structure of Pt<sub>3</sub>O<sub>4</sub>, where a network of metallic Pt-Pt bonds with very similar properties to Pt-Pt bonds in metallic platinum extends in all three crystallographic directions.

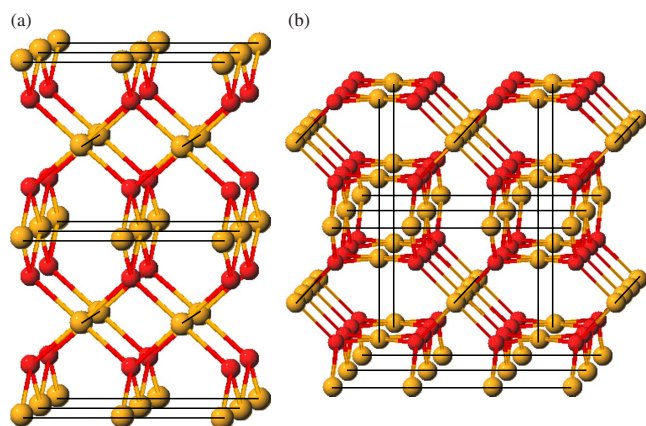


FIG. 4. (Color online) Pt-Pt bonds (black lines) in (a) PtO and (b) Pt<sub>3</sub>O<sub>4</sub>, as found by Bader analysis of the computed electron densities.

While a conclusive proof of the metallic character of Pt<sub>3</sub>O<sub>4</sub> would require investigations at a more accurate level, these results may suggest that metallicity may be an intrinsic feature of the compound as a consequence of short Pt-Pt distances between infinite square-planar stacking of PtO<sub>4</sub> motifs combined with a noninteger formal valence of the Pt ions. This would be consistent with the prediction of metallicity and the measured high conductivity of  $M_x$ Pt<sub>3</sub>O<sub>4</sub> platinum bronzes.<sup>25–27</sup>

#### IV. PLATINUM OXIDE NANOSTRUCTURES

After the investigations on the properties of bulk platinum oxides presented in the first part of this paper, we now move on to study the effect of finite size on the thermodynamical stability of the various oxide phases. This is motivated by the fact that in the majority of the existing technological applications, most notably in catalysis, platinum and its oxides are present in the form of nanoscopic particles, whose size and shape have a considerable influence on their stability and functional properties. This is due partly to the poorly crystallized nature of the platinum oxides<sup>5,24</sup> and especially to the intrinsic interest in producing oxide samples with a large surface-to-volume ratio to increase their catalytic efficiency.

##### A. Nanoparticles

In general, shape and size of nanoparticles are the results of an interplay between energetic and kinetic factors.<sup>71,72</sup> In particular, the surface energy of particles plays an important role in the time evolution of sintering processes.<sup>73</sup> In a first approximation, one can consider each particle as being isolated from the others (so that its number of Pt atoms is constant) and in thermodynamic equilibrium with the atmosphere environment, considered as an oxygen reservoir.

Under these assumptions, the equilibrium shape of a nanoparticle can be estimated by means of the Wulff's construction<sup>41</sup> from the calculated surface energies of different crystallographic terminations. This approach relies on the fact that, if a particle is large enough, the energy of zero-dimensional and one-dimensional defects (i.e., of vertices

and edges) can be neglected, and the particle's equilibrium shape at a given volume is the one that minimizes the total surface energy. For instance, in the case of Cu, it has been shown using empirical potentials that the Wulff's polyhedron (a truncated octahedron) indeed presents the lowest total energy per atom for particles with more than  $\sim 2500$  atoms, corresponding to a particle size of 3.8 nm.<sup>74</sup> In smaller particles, the effect of edges becomes important, and the preferred shape is an icosahedron with (111) faces.<sup>74,75</sup>

By using the surface energies  $\gamma$  previously calculated and reported in Ref. 29, we have determined the Wulff's particle shape in the case of Pt and Pt<sub>3</sub>O<sub>4</sub>. As reported in Ref. 29, for each facet, different possible terminations have been considered, as well as possibility of surface oxygen vacancy formation. The Wulff's polyhedron of metallic Pt is a truncated octahedron, where irregular hexagons with (111) orientation ( $\gamma=103$  meV/Å<sup>2</sup>) share the short edges with (100) squares ( $\gamma=131$  meV/Å<sup>2</sup>). The ratio between long and short edges is 1.58, and the surface fraction with (100) orientation is 14%. The Wulff's polyhedron of Pt<sub>3</sub>O<sub>4</sub> is a simple cube oriented along the principal axis of the crystal structure, since the surface energy of the (100) surface is much smaller than that of other crystallographic orientations, in particular, (110), both for Pt-terminated (128 vs 187 meV/Å<sup>2</sup>) and O-terminated surfaces (27 vs 77 meV/Å<sup>2</sup>). The third stable platinum oxide phase,  $\alpha$ -PtO<sub>2</sub>, is a particular case due to its peculiar layered structure and the resulting very small surface energy of the (0001) surface. In this case, isolated O-Pt-O trilayers can be considered as stand-alone "particles."

Given the particle shapes described above, we can now compute the Gibbs free energy of Pt, Pt<sub>3</sub>O<sub>4</sub>, and  $\alpha$ -PtO<sub>2</sub> particles with the same number of atoms from their relative volume and surface energy contributions according to the following formula:

$$\Delta G_{particle} = N_{Pt} \left( g_{PtO_x}^{bulk} - g_{Pt}^{bulk} - \frac{x}{2} g_{O_2}^{gas} \right) + \left( \sum_i A_i \gamma_i^{PtO_x} - \sum_j A_j \gamma_j^{Pt} \right), \quad (2)$$

where  $g$  is the Gibbs free energy per Pt atom of each phase,  $A$  is the surface area, and the sums over  $i$  and  $j$  run over the different crystallographic orientations of the surfaces present in PtO<sub>x</sub> and Pt particles, respectively. The obtained values of  $\Delta G_{particle}$  at a given oxygen partial pressure and at different temperatures can be now compared to determine the thermodynamic stability regions of oxidized particles. We find that the finite size of the particles has a considerable impact on the temperatures at which the  $\alpha$ -PtO<sub>2</sub>  $\rightarrow$  Pt<sub>3</sub>O<sub>4</sub> and Pt<sub>3</sub>O<sub>4</sub>  $\rightarrow$  Pt transitions take place. The results are summarized in Fig. 5 for an oxygen partial pressure of 1 atm taking into account particle sizes for which the Wulff's polyhedra can be considered as a reasonable approximation to the actual particle shape.

With respect to the phase diagram of the bulk phases (see Ref. 29), we find that with decreasing particle size, the stability region of  $\alpha$ -PtO<sub>2</sub> expands to higher temperatures at the expense of the stability region of Pt<sub>3</sub>O<sub>4</sub>. For relatively small particles, the influence of finite size on the transition tem-

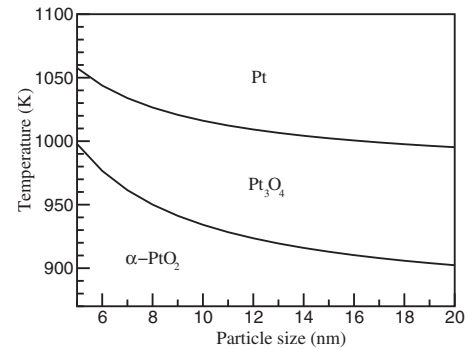


FIG. 5. Phase transition temperatures as function of Pt particle size at 1 atm oxygen pressure. The particle size is defined as the distance between two opposite (100) faces in a metallic Wulff's nanoparticle.

peratures appears to be surprisingly strong. This result is particularly important in view of the previously found peculiar catalytic activity of Pt<sub>3</sub>O<sub>4</sub> toward the oxidation of carbon compounds.<sup>29</sup> If the particle size distribution is broad enough, there will be a considerable amount of  $\alpha$ -PtO<sub>2</sub> (which we found to be catalytically inactive in the absence of defects<sup>29</sup>) forming also at temperatures for which the catalytically active Pt<sub>3</sub>O<sub>4</sub> phase is expected to be the most stable in the bulk form. This highlights the importance of achieving nearly monodispersed nanoparticle distributions in order to optimize their catalytic properties.

### B. $\alpha$ -PtO<sub>2</sub> nanotubes

Despite the expected inactivity of nondefective  $\alpha$ -PtO<sub>2</sub> toward the oxidation of carbon compounds, its catalytic properties in a number of other cases are intriguing. In fact,  $\alpha$ -PtO<sub>2</sub> has been found to be a potent catalyst for hydrosilylation reactions<sup>9</sup> and can catalyze the oxidation of ethanol to acetic acid in the presence of air.<sup>11</sup> It is thus very desirable to produce  $\alpha$ -PtO<sub>2</sub> samples with very large specific surface, which would maximize the number of catalytically active sites. To this aim,  $\alpha$ -PtO<sub>2</sub> particles with nanoscopic sizes were recently produced by one of the authors.<sup>11</sup> A transmission electron microscopy (TEM) analysis of the obtained products revealed the formation of needlelike  $\alpha$ -PtO<sub>2</sub> crystals with a diameter of roughly 6 nm and a length of roughly 50 nm.<sup>11</sup> Here, we report in Fig. 6 the results of a higher resolution TEM study on the same specimens, both as produced and after annealing at 350 °C in a nitrogen atmosphere. Irrespective of the annealing step, the samples investigated contained single dioxide layers partially curled and rolled up into needlelike structures (Fig. 6).

The peculiar appearance of these samples, combined with the graphitelike crystal structure of  $\alpha$ -PtO<sub>2</sub>, indicates that the formation of platinum dioxide nanotubes may be, in principle, possible. Nanotubes can be indeed fabricated by chemical processes in the case of TiO<sub>2</sub> (Refs. 76–78) and V<sub>2</sub>O<sub>5</sub>.<sup>79</sup> The latter compound is another example of oxide composed by compact layers held together by van der Waals forces.<sup>80,81</sup> The interest of nanotube oxide structures lies above all in the larger accessible specific surface with respect

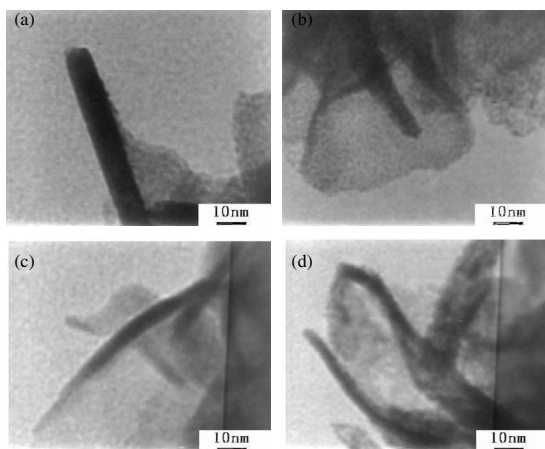


FIG. 6. HRTEM images of  $\alpha$ -PtO<sub>2</sub> specimens (at 100 keV). [(a) and (b)]  $\alpha$ -PtO<sub>2</sub> specimen as produced in Ref. 11; [(c) and (d)] similar specimen after annealing for 3 h at 350 °C in a N<sub>2</sub> atmosphere.

to nanoparticles [up to five times in the case of TiO<sub>2</sub> (Ref. 77)], which, in general, leads to an enhancement of the catalytic efficiency.

To investigate whether the formation of  $\alpha$ -PtO<sub>2</sub> nanotubes could be energetically feasible, we have performed a series of DFT calculations on single  $\alpha$ -PtO<sub>2</sub> layers rolled up into tubular structures of increasing diameter, with their axis along a Pt-Pt nearest neighbor bond (Fig. 7). In the calculations, periodic boundary conditions were applied to obtain infinite tubes along the principal axis and a separation between the periodically repeated tubes of at least 8 Å in all cases. In Fig. 8, we report the obtained total energy per formula unit of the tubes as a function of the tube radius  $r$  (which is defined by the distance between the Pt layer and the center of the tube in the plane perpendicular to the tube axis) both before and after structural relaxation. In the case of unrelaxed structures, we obtain a continuous curve which can be fitted by a power function  $E \sim r^{-2}$ , which is typical of, e.g., carbon nanotubes.<sup>82</sup> After full structural relaxation of

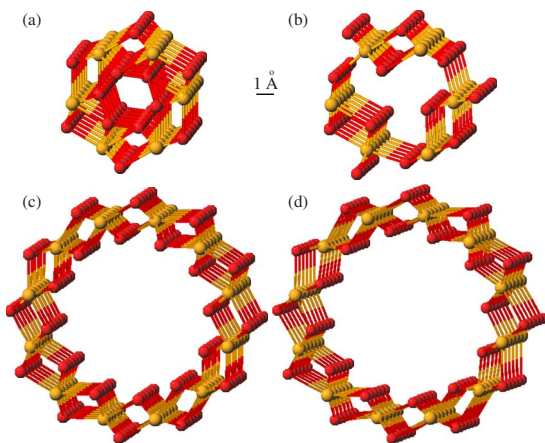


FIG. 7. (Color online)  $\alpha$ -PtO<sub>2</sub> nanotubes. Nanotube with six Pt atoms in the unit cell, (a) nonrelaxed and (b) relaxed; nanotube with 12 Pt atoms in the unit cell, (c) nonrelaxed and (d) relaxed.

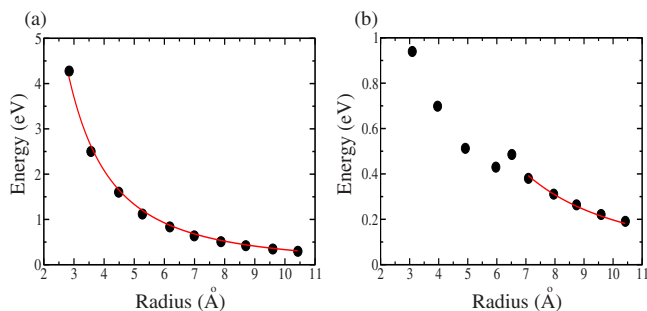


FIG. 8. (Color online) Formation energies of  $\alpha$ -PtO<sub>2</sub> nanotubes of increasing radius. (a) Unrelaxed system: circles, DFT results; solid line, fitted function  $\frac{\alpha}{r^2}$ , with  $\alpha=33.31$  eV Å<sup>2</sup>. (b) Relaxed system: circles, DFT results; solid line, fitted function  $\frac{\alpha}{r^2}$ , with  $\alpha=19.70$  eV Å<sup>2</sup>. Notice the different energy scales in the two diagrams.

the atomic positions, two different behaviors are obtained for radii larger or smaller than  $\sim 7$  Å (see Fig. 7). Larger tubes maintain their rolled-up PtO<sub>2</sub> layer structure upon relaxation, and the tube's radius slightly expands (e.g., from 7.88 to 7.96 Å in the case of the nanotube with 18 f.u.). Instead, the structural relaxation of smaller tubes leads to spontaneous breaking of Pt-O bonds and ejection of half of the oxygen atoms initially present in the inner side of the tube to the outer side [Figs. 7(a) and 7(b)]. The relaxation of a tube with a radius of about 6 Å (corresponding to 12 f.u. PtO<sub>2</sub> along the circumference) presents an intermediate behavior. In the lowest energy structure, which can be reached starting initially from a configuration like in Fig. 7(b), only one-fourth of the formula units remain with uncoordinated O atoms outside the tube. These different behaviors result in a discontinuity in the energy vs radius curve (Fig. 8). However, the values on the right side of the discontinuity can still be fitted with a power function  $E \sim r^{-2}$ , as shown in Fig. 8.

The computed values of total energy per formula units,  $E$ , at different radii (as reported in Fig. 8) can be related to the work per unit of length,  $W$ , required to form a circular tube starting from an initially planar sheet by

$$W a_0 = E N_{fu}, \quad (3)$$

where  $N_{fu}$  is the number of formula units in the elementary cell of the nanotube and  $a_0$  is the length of the elementary cell along the axis of the tube (3.14 Å in our case). In the case of a continuous elastic plate of small thickness  $h$  and elastic modulus  $G$ , the bending moment per unit of length is  $M = (Gh^3)/(12R)$ , where  $R$  is the radius of curvature upon bending.<sup>83</sup> Upon bending, a plate of edge length  $L$  will assume the form of an arc of angle  $\alpha = L/R$ . Therefore, the energy  $W$  required to form a circular tube of radius  $r = L/2\pi$  can be calculated by a simple integration of  $M$  along the angular coordinate  $\alpha$ :

$$W = \int_0^{2\pi} M(\alpha) d\alpha = \int_0^{2\pi} \frac{Gh^3}{12L} \alpha d\alpha = \frac{Gh^3 \pi}{12r}. \quad (4)$$

Since  $N_{fu}$  is proportional to the radius of the tube, the energy per formula unit,  $E$ , is proportional to  $W/r$ . Therefore, if the

energy stored in a nanotube obtained by rolling up a planar structure results from linear elasticity, then we expect a relationship  $E \sim r^{-2}$ , as obtained in our calculations and reported in Fig. 8.

We can now calculate the elastic modulus of a planar  $\text{PtO}_2$  sheet either from first principles by linear response theory (obtaining a value of 259 GPa) or from Eqs. (3) and (4) using the coefficient of the fitted curve in Fig. 8(b). A difficulty here is posed by the choice of the height  $h$ , which is not well determined in the case of  $\alpha\text{-PtO}_2$  layers. We have used two limit values of  $h$ , the first corresponding to the height difference between the oxygen atoms above and below the Pt plane (1.90 Å) plus twice the covalent radius of oxygen (given by half of the O-O distance in the oxygen molecule), i.e.  $h=3.11$  Å, and the second corresponding to the average experimental value of the height of the hexagonal unit cell of  $\alpha\text{-PtO}_2$ , i.e.,  $h=4.35$  Å. The values of  $G$  obtained are 197 GPa for  $h=3.11$  Å and 535 GPa for  $h=4.35$  Å. The value of 259 GPa obtained from first principles is nicely placed between these two limits, showing that elastic theory can indeed be used qualitatively to investigate the energetics of the platinum dioxide nanostructures considered here.

As a concluding remark for this section, we note that the calculated formation energy per formula unit of the  $\alpha\text{-PtO}_2$  nanotubes with respect to planar  $\alpha\text{-PtO}_2$  layers is as low as 0.2 eV for tubes with radii of about 1 nm. This value is comparable with the elastic energy stored in carbon nanotubes with a radius of 4 Å, which have been produced experimentally and are stable under normal conditions.<sup>82</sup> Thus, on the basis of our calculations, we suggest that the formation of small  $\alpha\text{-PtO}_2$  nanotubes, which could potentially find a number of applications in catalysis and nanotechnology, may be, in principle, possible. A way toward their experimental fabrication remains to be investigated and will probably require the presence of adequate nucleation centers (e.g., in the form of nanoparticles) and of carefully chosen chemical conditions.

The low energy required to bend the  $\alpha\text{-PtO}_2$  sheets is consistent with the presence of intriguing curled structures in the  $\alpha\text{-PtO}_2$  samples investigated via the TEM (Fig. 6). At the present stage, our results do not allow us to draw any firm conclusion about the driving force for the formation of the observed structures. However, it is known that the formation energy of oxygen vacancies in  $\alpha\text{-PtO}_2$  is relatively low (a values of 0.28 eV has been calculated in Ref. 36). We thus speculate that curling of planar O-Pt-O trilayers could be driven by the preferential clustering of vacancies on only one side of the layers during their formation.

## V. SUMMARY

The main results of our investigation into the physical properties of bulk and nanoscopic platinum oxide structures can be summarized as follows.

(1) At the GGA level,  $\alpha\text{-PtO}_2$  and  $\beta\text{-PtO}_2$  are found to be semiconductors with band energy gaps of 1.49 and 0.43 eV, respectively, as qualitatively predicted by ligand-field theory.

The electronic band structures of PtO and  $\text{Pt}_3\text{O}_4$  calculated at the GGA level present no gap between occupied and empty states. In the case of PtO, this appears to be an artifact of the local approximation to the exchange correlation and can be corrected at the GGA+ $U$  level, as indicated by opening of an energy gap at the  $M$  point of the Brillouin zone. This agrees with a recent calculation performed using an hybrid functional with exact exchange<sup>40</sup> and is qualitatively supported by ligand-field theory. However, in the case of  $\text{Pt}_3\text{O}_4$ , the computed electronic structure at the GGA+ $U$  level is still metallic. This seems to be consistent with the predicted metallic properties of a class of compounds of generic formula  $M_x\text{Pt}_3\text{O}_4$  (where  $M$  is an alkali or transition metal), the so-called platinum bronzes.<sup>25–27</sup> Metallicity of these compounds may originate from the noninteger formal valence of the Pt ions combined with the presence of infinite rows of direct Pt-Pt bonds along the three principal crystallographic directions, as found by means of a Bader analysis of the computed electron density.

(2) The effect of finite size on the relative thermodynamic stabilities of  $\text{PtO}_2$ ,  $\text{Pt}_3\text{O}_4$ , and Pt has been investigated taking into account Wulff's nanoparticles. With respect to the bulk phases,<sup>29</sup> we found that with decreasing particle size, the stability region of  $\alpha\text{-PtO}_2$  considerably expands to higher temperatures at the expense of the stability region of  $\text{Pt}_3\text{O}_4$ . Since in a previous work we have found that  $\text{Pt}_3\text{O}_4$  is very active toward the catalytic oxidation of carbon compounds, whereas  $\text{PtO}_2$  is fully inactive in the absence of defects, our results highlight the importance of achieving a nearly monodispersed distribution of particle sizes in order to optimize their catalytic properties.

(3) HRTEM images of  $\alpha\text{-PtO}_2$  samples reveal a very poorly crystalline material composed in large majority by thin  $\alpha\text{-PtO}_2$  sheets partially curled and rolled up into needle-like structures. This observation, combined with the graphitelike nature of  $\alpha\text{-PtO}_2$ , motivated us to investigate the energetic stability of  $\alpha\text{-PtO}_2$  nanotubes. We have found that the energy stored into a O-Pt-O trilayer rolled up into an infinite tube can be qualitatively estimated by elastic theory. Moreover, the small value of energy of formation of tubular structures with respect to planar sheets suggests that the fabrication of platinum dioxide nanotubes is energetically possible. This may also explain the spontaneous formation of the curled  $\alpha\text{-PtO}_2$  structures observed. We speculate that a driving force toward curling of planar O-Pt-O trilayers could be the preferential clustering of vacancies on only one side of the layers during their formation.

## ACKNOWLEDGMENTS

We would like to thank M. Bobeth, A. Ullrich, and A. De Vita for useful discussions and M. Stengel for his precious work of code development. We would like to thank U. Markwardt and the Centre for Information Services and High Performance Computing (ZIH) at the Dresden University of Technology for the outstanding technical support. Computing resources were provided by the Centre for Information Services and High Performance Computing of the Dresden University of Technology, Germany, and by the HPCx com-

puting facilities through the UKCP Consortium, UK. N.S. is grateful to the Theory of Condensed Matter Group at the Cavendish Laboratory, Cambridge for its hospitality in August 2003 and October 2004. L.C.C. acknowledges support by the Alexander von Humboldt Stiftung and by the

Deutschen Forschungsgemeinschaft within the Emmy-Noether Programme (Grants No. CI 144/1-1 and No. CI 144/2-1). This work has been financially supported by the German Federal Ministry of Education and Research (BMBF) within the project BIODADS.

\*nicola.seriani@univie.ac.at

- <sup>1</sup>J. M. Jørgensen, *J. Prakt. Chem.* **16**, 344 (1877).
- <sup>2</sup>W. J. Moore and L. Pauling, *J. Am. Chem. Soc.* **63**, 1392 (1941).
- <sup>3</sup>J. Waser and E. D. McClanahan, *J. Chem. Phys.* **19**, 413 (1951).
- <sup>4</sup>N. A. Shishakov, *Sov. Phys. Crystallogr.* **2**, 677 (1957).
- <sup>5</sup>O. Muller and R. Roy, *J. Less-Common Met.* **16**, 129 (1968).
- <sup>6</sup>M. P. H. Fernandez and B. L. Chamberland, *J. Less-Common Met.* **99**, 99 (1984).
- <sup>7</sup>C.-B. Wang, H.-K. Lin, S.-N. Hsu, T.-H. Huang, and H.-C. Chiu, *J. Mol. Catal. A: Chem.* **188**, 201 (2002).
- <sup>8</sup>V. Voorhees and R. Adams, *J. Am. Chem. Soc.* **44**, 1397 (1922).
- <sup>9</sup>N. Sabourault, G. Mignani, A. Wagner, and C. Mioskowski, *Org. Lett.* **4**, 2117 (2002).
- <sup>10</sup>A. Hamze, O. Provot, M. Alami, and J.-D. Brion, *Org. Lett.* **7**, 5625 (2005).
- <sup>11</sup>J. Zhensheng, X. Chanjuan, Z. Qingmei, Y. Feng, Z. Jiazheng, and X. Jinzhen, *J. Mol. Catal. A: Chem.* **191**, 61 (2003).
- <sup>12</sup>N. I. Zakharchenko, *Russ. J. Appl. Chem.* **74**, 1686 (2001).
- <sup>13</sup>E. P. J. Mallens and J. H. B. J. Hoebink, *Catal. Lett.* **33**, 291 (1995).
- <sup>14</sup>B. L. M. Hendriksen and J. W. M. Frenken, *Phys. Rev. Lett.* **89**, 046101 (2002).
- <sup>15</sup>G. Jerkiewicz, G. Vatankhah, J. Lessard, M. P. Soriaga, and Y.-S. Park, *Electrochim. Acta* **49**, 1451 (2004).
- <sup>16</sup>F. B. Diniz and R. R. Ueta, *Electrochim. Acta* **49**, 4281 (2004).
- <sup>17</sup>Y. Abe, H. Yanagisawa, and K. Sasaki, *Jpn. J. Appl. Phys., Part 1* **37**, 4482 (1998).
- <sup>18</sup>K. Kuribayashi and S. Kitamura, *Thin Solid Films* **400**, 160 (2001).
- <sup>19</sup>T. Kikukawa, T. Nakano, T. Shima, and J. Tominaga, *Appl. Phys. Lett.* **81**, 4697 (2002).
- <sup>20</sup>T. Shima, T. Kikukawa, T. Nakano, and J. Tominaga, *Jpn. J. Appl. Phys., Part 1* **45**, 136 (2006).
- <sup>21</sup>H. Neff, S. Henkel, E. Hartmannsgruber, E. Steinbeiss, W. Michalke, K. Steenbeck, and H. G. Schmidt, *J. Appl. Phys.* **79**, 7672 (1996).
- <sup>22</sup>J. J. Blackstock, D. R. Stewart, and Z. Li, *Appl. Phys. A: Mater. Sci. Process.* **80**, 1343 (2005).
- <sup>23</sup>L. Maya, L. Riestler, T. Thundat, and C. S. Yust, *J. Appl. Phys.* **84**, 6382 (1998).
- <sup>24</sup>K. B. Schwartz and C. T. Prewitt, *J. Phys. Chem. Solids* **45**, 1 (1984).
- <sup>25</sup>D. Cahen, J. A. Ibers, and J. B. Wagner, *Inorg. Chem.* **13**, 1377 (1974).
- <sup>26</sup>R. D. Shannon, T. E. Gier, P. F. Garcia, P. E. Bierstedt, R. B. Flippen, and A. J. Vega, *Inorg. Chem.* **21**, 3372 (1982).
- <sup>27</sup>M.-L. Doublet, E. Canadell, and M.-H. Whangbo, *J. Am. Chem. Soc.* **116**, 2115 (1984).
- <sup>28</sup>D. Cahen and J. A. Ibers, *J. Catal.* **31**, 369 (1973).
- <sup>29</sup>N. Seriani, W. Pompe, and L. C. Ciacchi, *J. Phys. Chem. B* **110**, 14860 (2006).
- <sup>30</sup>X.-Q. Gong, R. Raval, and P. Hu, *Phys. Rev. Lett.* **93**, 106104 (2004).
- <sup>31</sup>W. X. Li, L. Österlund, E. K. Vestergaard, R. T. Vang, J. Matthiesen, T. M. Pedersen, E. Laegsgaard, B. Hammer, and F. Besenbacher, *Phys. Rev. Lett.* **93**, 146104 (2004).
- <sup>32</sup>W. X. Li and B. Hammer, *Chem. Phys. Lett.* **409**, 1 (2005).
- <sup>33</sup>J. G. Wang *et al.*, *Phys. Rev. Lett.* **95**, 256102 (2005).
- <sup>34</sup>M. D. Ackermann *et al.*, *Phys. Rev. Lett.* **95**, 255505 (2005).
- <sup>35</sup>R. Wu and W. H. Weber, *J. Phys.: Condens. Matter* **12**, 6725 (2000).
- <sup>36</sup>S. Zhuo and K. Sohlberg, *Physica B* **381**, 12 (2006).
- <sup>37</sup>K. C. Hass and A. E. Carlsson, *Phys. Rev. B* **46**, 4246 (1992).
- <sup>38</sup>K.-T. Park, D. L. Novikov, V. A. Gubanov, and A. J. Freeman, *Phys. Rev. B* **49**, 4425 (1994).
- <sup>39</sup>R. Ahuja, S. Auluck, B. Johansson, and M. A. Khan, *Phys. Rev. B* **50**, 2128 (1994).
- <sup>40</sup>J. Uddin, J. E. Peralta, and G. E. Scuseria, *Phys. Rev. B* **71**, 155112 (2005).
- <sup>41</sup>G. Wulff, *Z. Kristallogr.* **34**, 449 (1901).
- <sup>42</sup>J. P. Perdew and Y. Wang, *Phys. Rev. B* **45**, 13244 (1992).
- <sup>43</sup>N. Troullier and J. L. Martins, *Phys. Rev. B* **43**, 1993 (1991).
- <sup>44</sup>A. D. Vita, A. Canning, G. Galli, F. Gygi, F. Mauri, and R. Car, *EPFL Supercompt. J.* **6**, 22 (1994).
- <sup>45</sup>M. Stengel and A. De Vita, *Phys. Rev. B* **62**, 15283 (2000).
- <sup>46</sup>L. C. Ciacchi, W. Pompe, and A. D. Vita, *J. Am. Chem. Soc.* **123**, 7371 (2001).
- <sup>47</sup>L. C. Ciacchi, M. Mertig, W. Pompe, S. Meriani, and A. D. Vita, *Platinum Met. Rev.* **47**, 98 (2003).
- <sup>48</sup>H. J. Monkhorst and J. D. Pack, *Phys. Rev. B* **13**, 5188 (1976).
- <sup>49</sup>The ABINIT code is a common project of the Universite' Catholique de Louvain and Corning Incorporated and other contributors (<http://www.abinit.org>).
- <sup>50</sup>V. I. Anisimov, J. Zaanen, and O. K. Andersen, *Phys. Rev. B* **44**, 943 (1991).
- <sup>51</sup>V. I. Anisimov, F. Aryasetiawan, and A. I. Lichtenstein, *J. Phys.: Condens. Matter* **9**, 767 (1997).
- <sup>52</sup>S. Baroni, A. dal Corso, S. de Gironcoli, P. Giannozzi, C. Cavazzoni, G. Ballabio, S. Scandolo, G. Chiarotti, P. Focher, A. Pasquarello, K. Laasonen, A. Trave, R. Car, N. Marzari, and A. Kokalj, <http://www.pwscf.org/>
- <sup>53</sup>D. Vanderbilt, *Phys. Rev. B* **41**, 7892 (1990).
- <sup>54</sup>G. Kresse, A. Gil, and P. Sautet, *Phys. Rev. B* **68**, 073401 (2003).
- <sup>55</sup>L. Köhler and G. Kresse, *Phys. Rev. B* **70**, 165405 (2004).
- <sup>56</sup>K. Reuter and M. Scheffler, *Phys. Rev. Lett.* **90**, 046103 (2003).
- <sup>57</sup>Y. Abe, M. Kawamura, and K. Sasaki, *Jpn. J. Appl. Phys., Part 1* **38**, 2092 (1999).
- <sup>58</sup>A. Punnoose, M. S. Seehra, and I. Wender, *Fuel Process. Technol.* **74**, 33 (2001).
- <sup>59</sup>K. L. Saenger, C. Cabral, Jr., C. Lavoie, and S. M. Rossnagel, *J.*

- Appl. Phys. **86**, 6084 (1999).
- <sup>60</sup>J. R. McBride, G. W. Graham, C. R. Peters, and W. H. Weber, J. Appl. Phys. **69**, 1596 (1991).
- <sup>61</sup>W. H. Weber, G. W. Graham, and J. R. McBride, Phys. Rev. B **42**, 10969 (1990).
- <sup>62</sup>M. Hasegawa and K. Nishidate, Phys. Rev. B **70**, 205431 (2004).
- <sup>63</sup>Y. Baskin and L. Meyer, Phys. Rev. **100**, 544 (1955).
- <sup>64</sup>L. E. Orgel, *An Introduction to Transition Metal Chemistry: Ligand-Field Theory* (Butler & Tanner, London, 1960).
- <sup>65</sup>To be precise, at  $U=9$  eV, the ground state is spin polarized with  $\sim 0.24$  Bohr magnetons per Pt atom. However, the nonpolarized solution lies only 0.5 meV/f.u. above the spin-polarized solution.
- <sup>66</sup>R. F. W. Bader, *Atoms in Molecules: A Quantum Theory* (Oxford University Press, Oxford, 1990).
- <sup>67</sup>S. Jenkins, J. Phys.: Condens. Matter **14**, 10251 (2002).
- <sup>68</sup>R. Laskowski, P. Blaha, and K. Schwarz, Phys. Rev. B **67**, 075102 (2003).
- <sup>69</sup>W. Jauch and M. Reehuis, Phys. Rev. B **67**, 184420 (2003).
- <sup>70</sup>Y. A. Abramov, Acta Crystallogr., Sect. A: Found. Crystallogr. **A53**, 264 (1997).
- <sup>71</sup>J. M. Petroski, Z. L. Wang, T. C. Green, and M. A. El-Sayed, J. Phys. Chem. B **102**, 3316 (1998).
- <sup>72</sup>F. Baletto and R. Ferrando, Rev. Mod. Phys. **77**, 371 (2005).
- <sup>73</sup>C. T. Campbell, S. C. Parker, and D. E. Starr, Science **298**, 811 (2002).
- <sup>74</sup>D. Reinhard, B. D. Hall, P. Berthoud, S. Valkealahti, and R. Monot, Phys. Rev. Lett. **79**, 1459 (1997).
- <sup>75</sup>S. Valkealahti and M. Manninen, Phys. Rev. B **45**, 9459 (1992).
- <sup>76</sup>T. Kasuga, M. Hiramatsu, A. Hoson, T. Sekino, and K. Niihara, Langmuir **14**, 3160 (1998).
- <sup>77</sup>T. Kasuga, M. Hiramatsu, A. Hoson, T. Sekino, and K. Niihara, Adv. Mater. (Weinheim, Ger.) **11**, 1307 (1999).
- <sup>78</sup>D. Gong, C. A. Grimes, O. K. Varghese, W. Hu, R. S. Singh, Z. Chen, and E. C. Dickey, J. Mater. Res. **16**, 3331 (2001).
- <sup>79</sup>Y. Wang and G. Cao, Chem. Mater. **18**, 2787 (2006).
- <sup>80</sup>J. Y. Kempf, B. Silvi, A. Dietrich, C. R. A. Catlow, and B. Margret, Chem. Mater. **5**, 641 (1993).
- <sup>81</sup>V. Brázdová, M. V. Ganduglia-Pirovano, and J. Sauer, Phys. Rev. B **69**, 165420 (2004).
- <sup>82</sup>D.-H. Oh and Y. H. Lee, Phys. Rev. B **58**, 7407 (1998).
- <sup>83</sup>S. Timoshenko and J. M. Gere, *Mechanics of Materials* (Brooks-Cole, Belmont, MA, 1984), p. 284.